Electronic Supplementary Material (ESI) for ChemComm.

Supporting information

for

Iron partially occupied sulfur vacancies in WS_2 boosts the electrochemical nitrogen fixation at low potential

Jiuxiao Sun[a#], Xue Li[a#], Tiantian Xiong[b], Ying Ling[b*] and Zehui Yang[b,c*]

[a]State Key Laboratory for Hubei New Textile Materials and Advanced Processing Technology, School of Materials Science and Engineering, Wuhan Textile University, 430200 Wuhan, P. R. China.

[b]Sustainable Energy Laboratory, Faculty of Materials Science and Chemistry, China University of Geosciences Wuhan, 388 Lumo RD, Wuhan, 430074, P. R. China.

[c]Zhejiang Institute, China University of Geosciences, Hangzhou, 311305, P. R. China.

#Jiuxiao Sun and Xue Li equally contributed to this work.

Preparation of WS_2: Firstly, AMT (0.97 g) was dissolved to deionized water (15 mL). The compound was stirred for 10 min to form a transparent, homogeneous solution at room temperature. According to the ratio of W:S=1:10, 17 mL of ammonium thiosulphate solution (8 wt%) was added. The resultant solution was heated to 70 ^{o}C for 1 h. After cooling to the room temperature, 270 mL of hydrochloric acid is slowly added to generate H_2S gas. The reaction was terminated until the solution turned to reddish brown. The resultant solution was centrifuged three times and the precipitation was placed in a blower dryer at 50 ^{o}C for 5 h. The precursor was ground into a uniform grain size of powder and placed in the tube furnace with Ar/H_2 flow for 30 min. After changing to air flow (60 mL min^{-1}), the precursor was heated to 450 ^{o}C for 4 h (5 ^{o}C min^{-1}). The WS_2 template was obtained. Finally, the pure WS_2 nanosheets can be obtained by removing the WO_3 template with 0.1 M NaOH solution.

Synthesis of Fe-WS_2: $Fe(NO_3)_3$ and WS_2 were dispersed in water and the mixture was heated to evaporate water. The powder was heated to 450 ^{o}C with Ar/H_2 flow for 2 h. Finally, Fe-WS_2 was obtained.

Material characterization: The morphologies and microstructures of the samples were observed by a scanning electron microscope (SEM) at an accelerating voltage of 5 kV (SU8010, HITACHI, Japan). Energy dispersive spectroscopy (EDS) analysis was performed at the acceleration voltage of 200 kV using a TECNAI G2 F20 (FEI Ltd., USA) TEM equipped with a Bruker X

Flash 5030 detector (Bruker Nano GmbH, Berlin, Germany). N_2 adsorption property measurements were conducted on a temperature-programmed desorption (TPD) apparatus Micromeritics ASAP 2020 using helium as carrier gas, and the adsorbed amount was calculated from thermal conductivity signals. X-ray photoelectron spectroscopy (XPS, ESCALAB 250Xi) were used to investigate the surface composition of samples. The electro-catalyst powder was placed on indium substrate and measured under high vacuum atmosphere. During the calibration process set C1s peak was fixed at 284.5 eV as standard. The absorbance data of spectrophotometer were recorded on SPECORD PIUS200 UV-vis spectrophotometer. NMR was performed on Bruker AVANCE III HD 400 instrument.

Electrochemical measurement: All electrochemical testing were recorded at room temperature using the Reference 1000 Gamry. The electrochemical testing was accomplished in a three-electrode system. Glassy carbon electrode with a diameter of 3 mm (GCE) and a saturated calomel electrode (SCE) and a carbon rod were used as working, reference and counter electrodes. The catalyst loading was controlled to be 0.285 mg cm^{-2}. NRR electrocatalytic activity was carried out in a N_2 saturated 0.05 M H_2SO_4 solution in an H-type electrochemical cell, which was separated by a Nafion 211 membrane. Nitrogen gas was purified by 0.5 M H_2SO_4 before purging into electrolyte. The membrane was boiled in ultrapure water for 1 h, then heated to 80 °C in H_2O_2 (5 %) for 1 h and finally boiled in sulfuric acid (0.5 M) for 2 h. All the potentials in this manuscript were converted to the RHE reference scale using E (vs.

RHE) = E (vs. SCE) + 0.0591 × pH + 0.244 V.

Ammonia calculation: NRR electrolysis experiment was tested in 0.05 M H_2SO_4 and the NH_3 concentration was spectrophotometrically determined by the method of indophenol blue. 2 mL of electrolyte was obtained from the cathodic chamber and then added 1 M NaOH solution containing 5% salicylic acid and 5% sodium citrate to the electrolyte. Thereafter, 1 mL of 0.05 M NaClO and 0.2 mL of 1% sodium nitroprusside were added to the above solution. The UV-vis absorption spectrum was measured at 655 nm. The NH_3 accumulation-absorbance curves were plotted with a list of concentration of standard NH_3 solution. It showed an excellent linear relationship between the absorbance value and the $(NH_4)_2SO_4$ concentration from the fitting curve. The baseline of UV-vis spectroscopy was recorded before measuring the electrolyte after NRR catalysis.

FE and NH_3 yield rate: The FE of nitrogen reduction reaction was evaluated as the amount of electric charge used for synthesizing NH_3 divided the total charge passed through the electrodes during the electrolysis. The total amount of NH_3 produced during NRR electrolysis experiments was measured using colorimetric methods. Assuming three electrons were needed to form a NH_3 molecule, the FE calculation was described as follow:

$$FE=(3\times F\times C_{NH3}\times V)\times(17\times Q)^{-1}$$

The rate of NH_3 formation (V_{NH3}) can be measured using the following equation:

$$V_{NH3}=C_{NH3}\times V\times(t\times m_{cat})^{-1}$$

F represents the Faraday constant, C_{NH3} is the measured amount of NH_3 accumulation,

V is cathode chamber electrolyte volume, t is the NRR testing time and m_{cat} is the catalyst loading on the electrode.

Nuclear magnetic resonance (NMR) spectroscopy: In the electrocatalytic nitrogen reduction experiment, Argon gas was purged to the cathodic cell to remove impurity gas and then purging for 30 min with the gas to be tested. After electrolysis at -0.15 V vs. RHE for 2 h, 50 mL of the electrolyte was taken out and acidized to pH 3 by adding H_2SO_4 (pH=1), and then concentrated to 5 mL by heating via reduced pressure distillation. Afterwards, 0.55 mL of the resulting solution was taken out and mixed with 0.05 mL D_2O for ^{1}H-NMR measurement. A total of 1024 transient scans were recorded with an inter-scan delay of 1 s. 64 K complex points was acquired for each FID with an acquisition time of 3.4 s. The produced ammonia was quantitatively detected by using ^{1}H-NMR means on a Bruker AVANCE III HD 400 instrument. A known amount of D_2O was used as an internal standard. By analyzing the acquired spectra, $^{15}NH_4^+$ calibration curve was obtained by integrating the ammonia signal appeared at 7.00 ppm as a function of prepared known $(^{15}NH_4)_2SO_4$ (from Aladdin) standard solution dissolved in 0.05 M H_2SO_4.

Computational study: The calculations were performed with the VASP package, using the Perdew-Burke-Ernzerhof (PBE) approximation of density functional theory (DFT) to describe the exchange-correlation interactions and the projector augmented wave (PAW) method to account for core-valence interactions. The energy cutoff for plane wave expansions was set to 400 eV, and the reciprocal space was sampled by a 2×2×1 grid which is generated by VASPKIT. At least 15 Å vacuum layer was applied

in the z-direction of the slab models to prevent the vertical interactions between slabs. All structures were fully relaxed to the ground state and spin-polarization was considered in all calculations. The convergence thresholds for structural optimization was set at 0.02 eV/Å in force and the convergence criterion for energy is 1×10^{-5} eV. The reaction Gibbs free energy changes (ΔG) for each step were based on the computational hydrogen electrode model and can be calculated using the following equation:

$$\Delta G = \Delta E + \Delta ZPE - T\Delta S + \Delta G_U + \Delta G_{pH} \quad (1)$$

Where ΔE is obtained directly from DFT calculations, ΔZPE is the change in zero-point energies (ZPE), T is the temperature (298.15 K), and ΔS is the change in entropy of products and reactants. $\Delta G_U = eU$ is the contribution of electrode potential to ΔG, and $\Delta G_{pH} = k_B T \ln 10 \times pH$, and the pH value in this calculation was set to zero. The overpotential η for N_2 reduction reactions is obtained by,

$$\eta = U_{equilibrium} - U_{limiting} \quad (2)$$

where $U_{equilibrium}$ is the equilibrium potential of the N_2 reduction process (0.16 V) and $U_{limiting}$ is obtained by $U_{limiting} = \Delta G_{max}/e$, in which, ΔG_{max} is the most positive ΔG of each elementary step of the whole process.

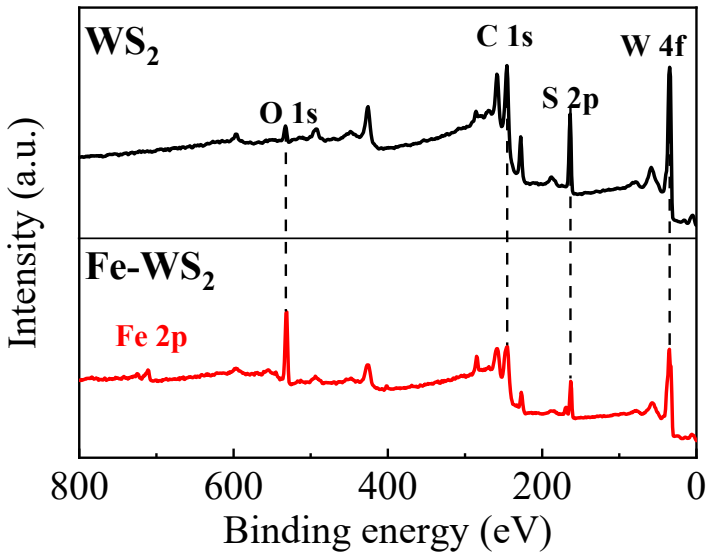

Figure S1 XPS survey scan of WS_2 and Fe-WS_2 electrocatalysts.

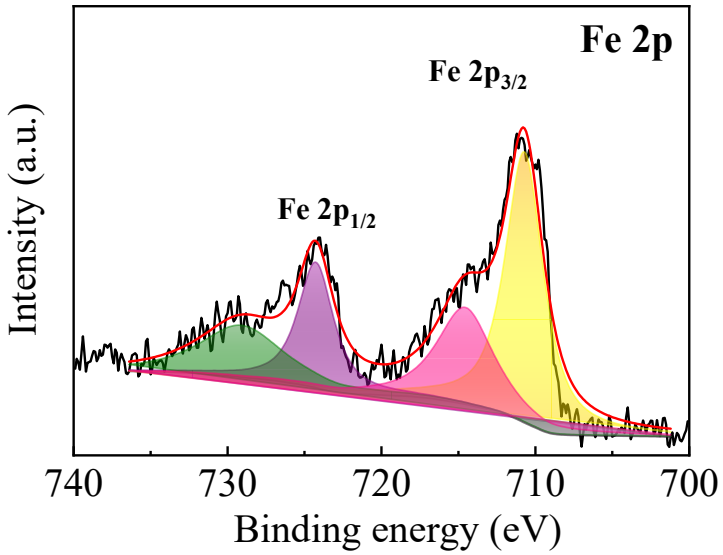

Figure S2 Deconvoluted Fe 2p peak of Fe-WS_2 electrocatalyst.

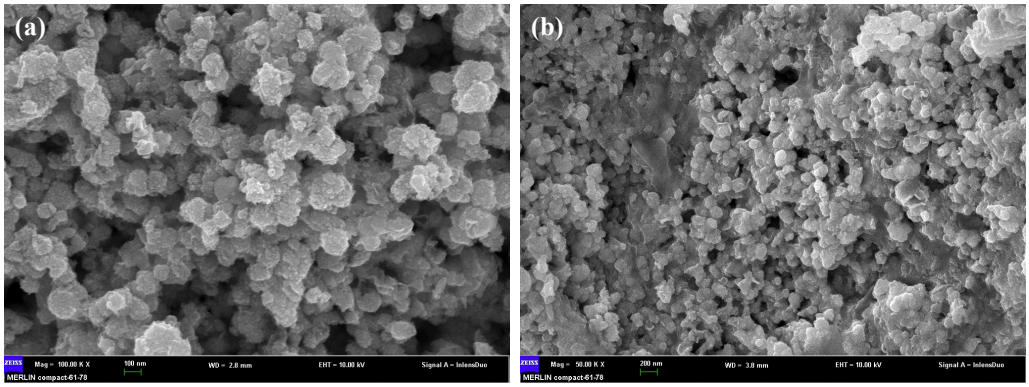

Figure S3 SEM images of WS_2 and Fe-WS_2 electrocatalysts.

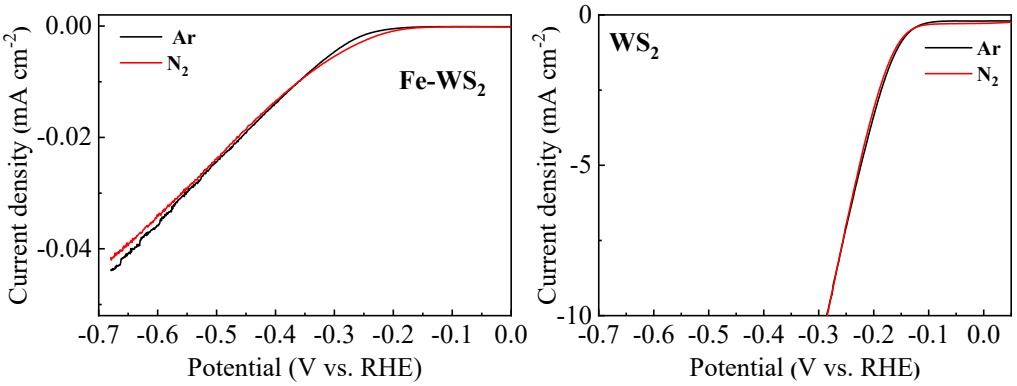

Figure S4 LSV curves of Fe-WS_2 and WS_2 electrocatalysts recorded in Ar- and N_2-saturated 0.05 M H_2SO_4 electrolyte.

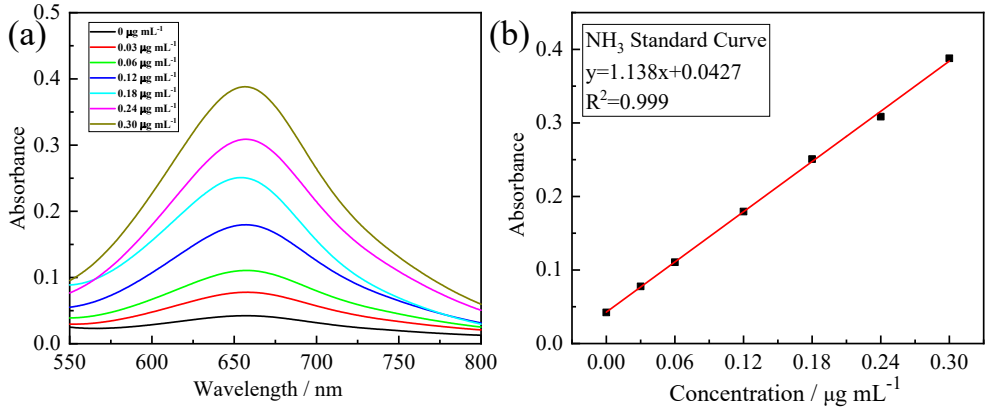

Figure S5 Standard curve for NH_3 based on intensities of UV-vis spectroscopies.

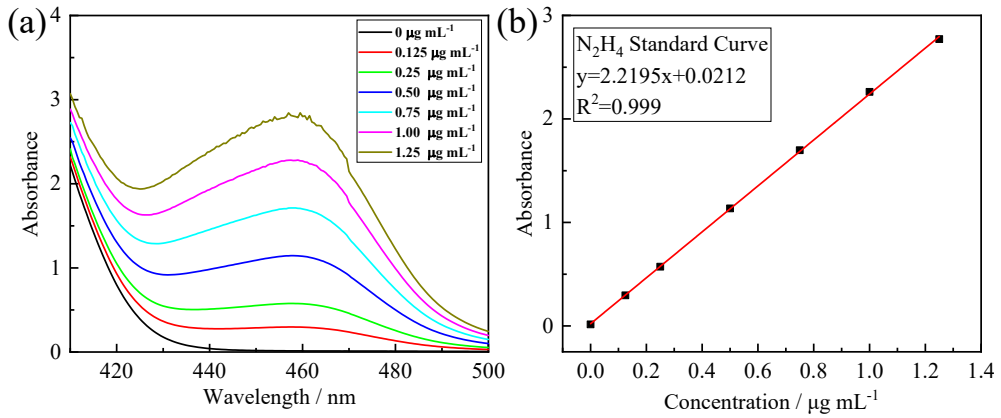

Figure S6 Standard curve for N_2H_4 based on intensities of UV-vis spectroscopies.

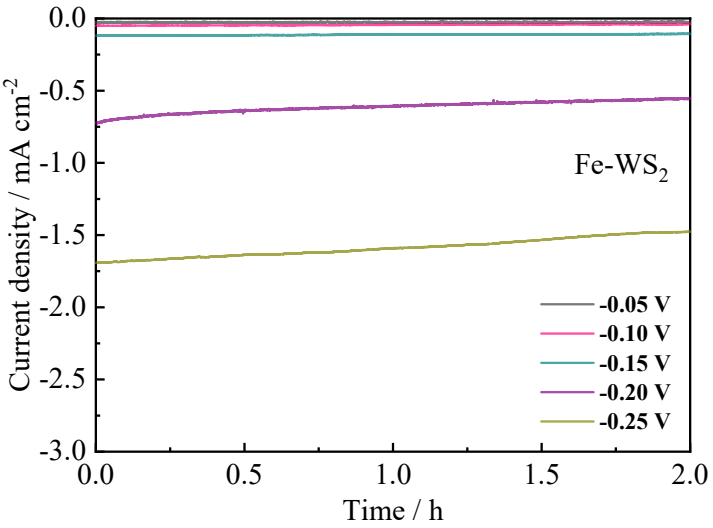

Figure S7 i-t test of Fe-WS_2 in N_2-saturated 0.05 M H_2SO_4 electrolyte at various potentials.

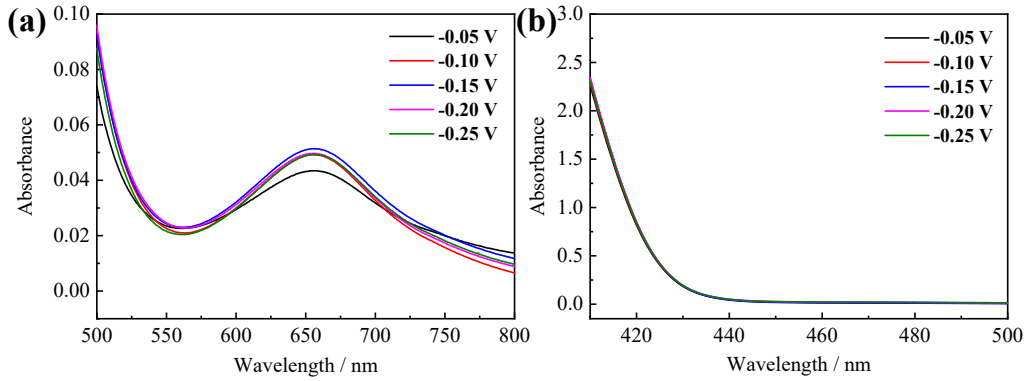

Figure S8 UV-vis spectroscopies of Fe-WS_2 at various potentials.

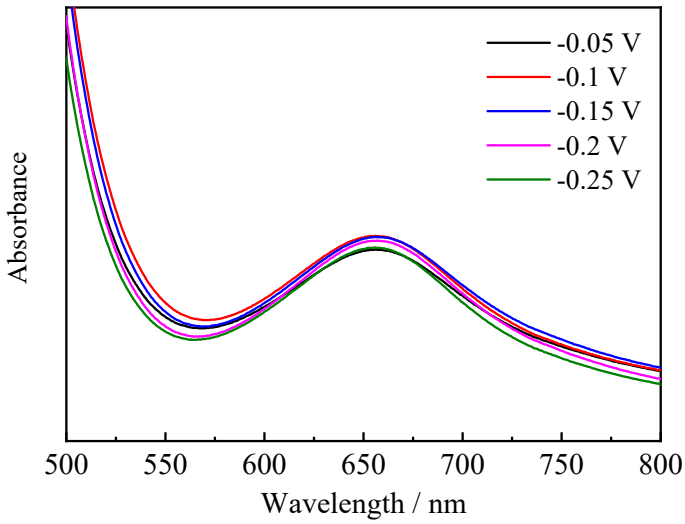

Figure S9 UV-vis spectroscopies of WS_2 at various potentials.

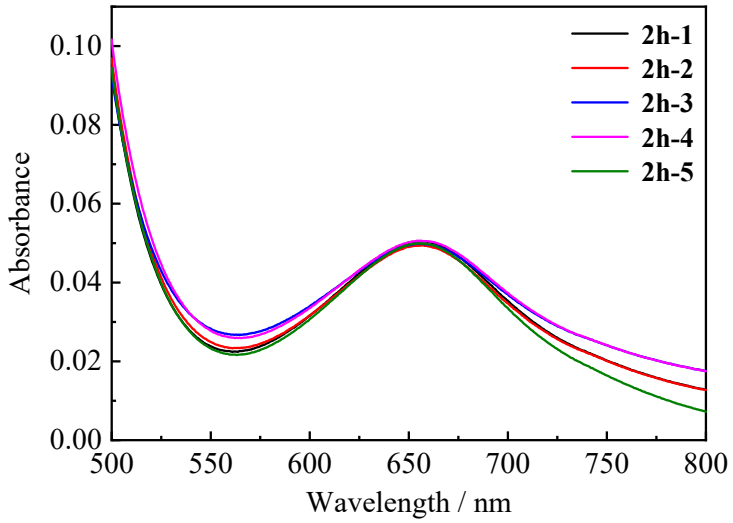

Figure S10 UV-vis spectroscopies of Fe-WS_2 at -0.1 V vs. RHE.

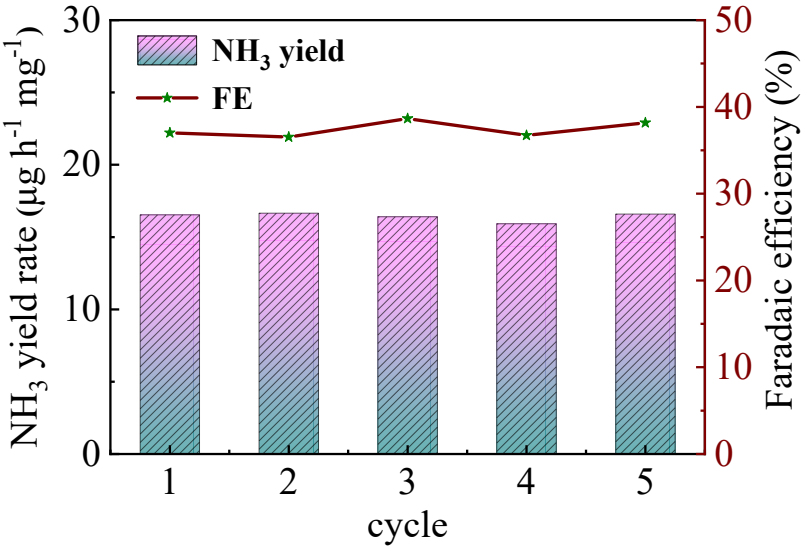

Figure S11 Faradaic efficiency and ammonia yield rate of Fe-WS_2 in 5 cycles.

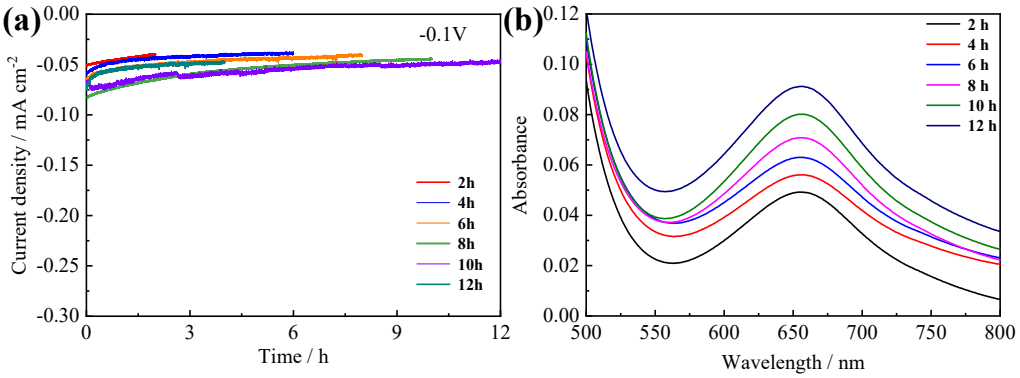

Figure S12 stability test and UV-vis spectroscopies of Fe-WS_2.

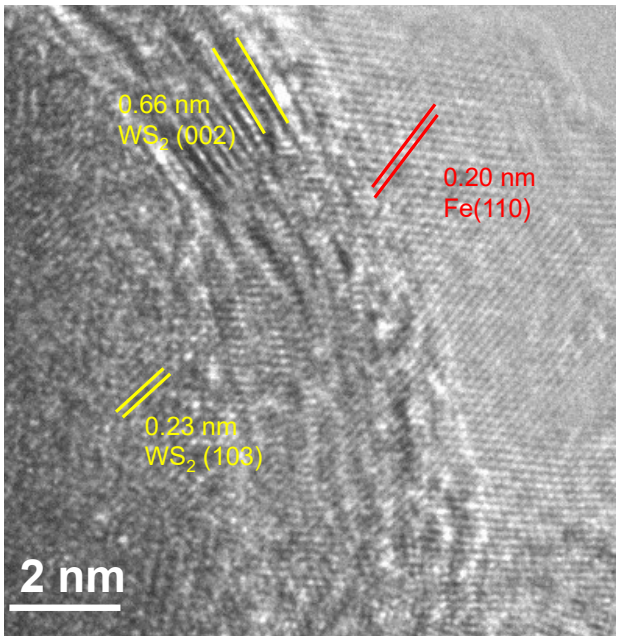

Figure S13 TEM images of Fe-WS2 after 12 h catalysis.

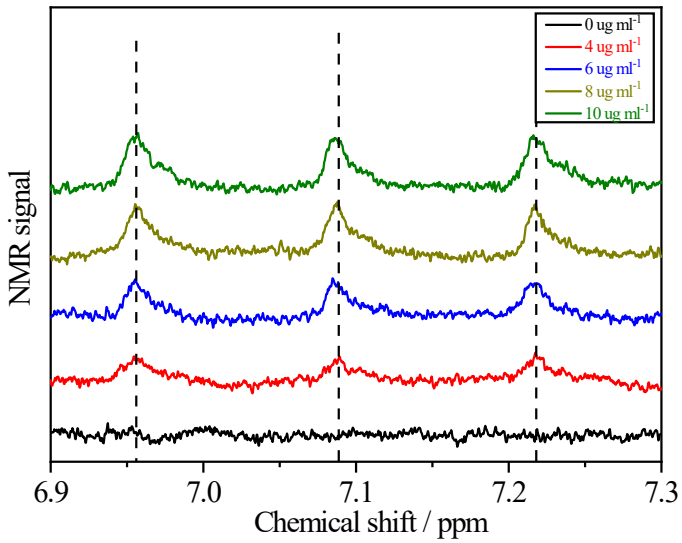

Figure S14 Standard curve for NH_3 based on intensities of NMR.

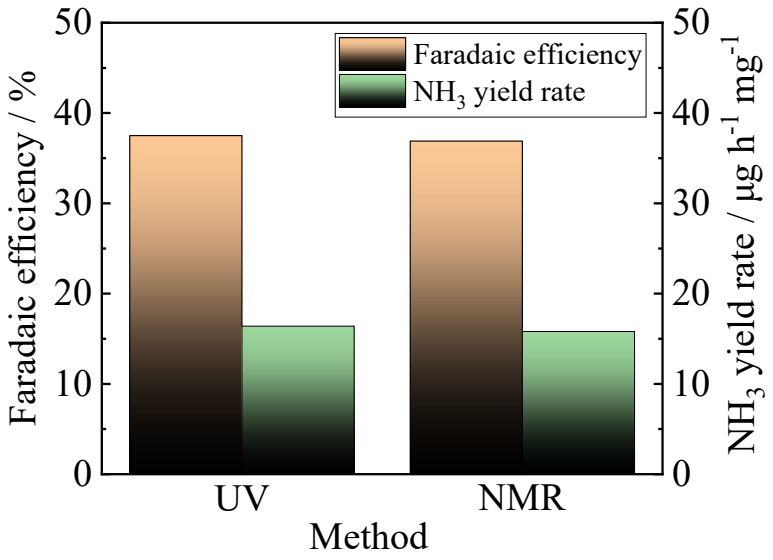

Figure S15 Comparison of Faradaic efficiency and ammonia yield rate from two different testing methods.

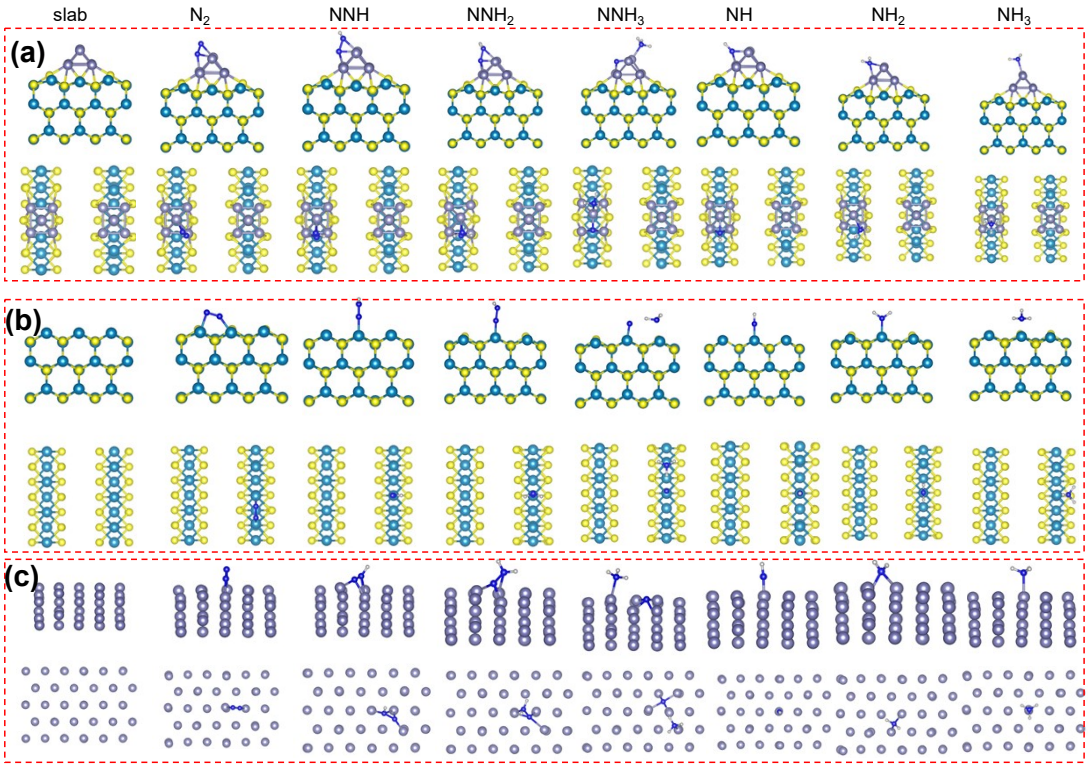

Figure S16 Adsorption of NRR intermediates on Fe-WS_2 (a), WS_2 (b) and Fe (c).

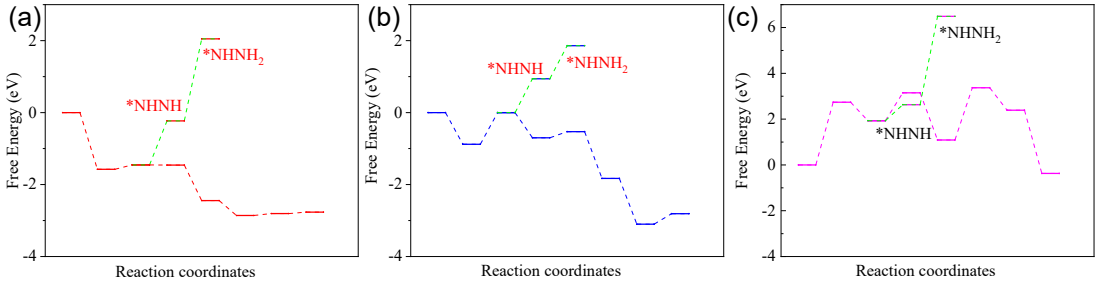

Figure S17 Free energy diagrams of NRR catalysis by Fe-WS_2 (a), WS_2 (b) and Fe (c) with different pathways.